Relation Between the Interannual Variability in the Stratospheric Rossby Wave Forcing and Zonal Mean Fields Suggesting an Interhemispheric Link in the Stratosphere

Yuki Matsushita[1], Daiki Kado[2], Masashi Kohma[1], and Kaoru Sato[1]

5 [1]Department of Earth and Planetary Science, the University of Tokyo, Tokyo, 113-0033, Japan
[2]Research Center for Advanced Science and Technology, the University of Tokyo, Tokyo, 153-8904, Japan

Correspondence to: Yuki Matsushita (matsushitayu@eps.s.u-tokyo.ac.jp)

Abstract. Focusing on the interannual variabilities in the zonal mean fields and Rossby wave forcing in austral winter, an interhemispheric coupling in the stratosphere is examined using reanalysis data: the Modern-Era Retrospective Analysis for

10 Research and Applications, version 2 (MERRA-2). In the present study, the Eliassen-Palm (EP) flux divergence averaged over the latitude and height regions of 50°–30°S and 0.3–1 hPa, respectively, are used as a proxy of the Rossby wave forcing, where the absolute value of the EP flux divergence is maximized in the winter in the Southern Hemisphere (SH). The interannual variabilities in the zonal mean temperature and zonal wind are significantly correlated with the SH Rossby wave forcing in the stratosphere in both the SH and Northern Hemisphere (NH). The interannual variability in the strength of the

15 poleward residual mean flow in the SH stratosphere is also correlated with the strength of the wave forcing. This correlation is significant even around the equator at an altitude of 40 km and at NH low latitudes of 20-40 km. The temperature anomaly is consistent with this residual mean flow anomaly. The relationship between the cross-equatorial flow and the zonal mean absolute angular momentum gradient ($\overline{M}_y$) is examined in the meridional cross section. The $\overline{M}_y$ around the equator at the altitude of 40 km is small when the wave forcing is strong, which provides a pathway for the cross-equatorial residual mean

20 flow. These results indicate that an interhemispheric coupling is present in the stratosphere through the meridional circulation modulated by the Rossby wave forcing.

1 Introduction

The Brewer-Dobson circulation (BDC) is composed of the residual mean circulation and isentropic mixing in the stratosphere. The deep branch of the BDC is mainly driven by planetary-scale Rossby waves on the winter hemisphere

25 (Butchart, 2014). The maximum tropical upwelling is observed on the summer hemisphere of the equatorial region (e.g., Plumb and Eluszkiewics, 1999; Tung and Kinersley, 2001; Okamoto et al., 2011). However, the Rossby wave forcing in the winter extratropics cannot directly drive the cross-equatorial flow, and a small angular momentum gradient around the equator is required to maintain the cross-equatorial flow (Plumb and Eluszkiewics, 1999). Tomikawa et al. (2008) used high-

resolution general circulation model (GCM) simulation data to show that the strong residual mean flow crosses the equator
30   along nearly horizontally aligned contours of absolute angular momentum $\bar{M}$.

Previous studies have highlighted the importance of Rossby waves in the stratospheric interannual variabilities from various
viewpoints, such as extratropical zonal winds in the winter modulated by the stratospheric quasi-biennial oscillation in the
Northern Hemisphere (NH) (Holton and Tan, 1980; Yamashita et al., 2011) and Southern Hemisphere (SH) (Baldwin and
Dunkerton, 1998), the location of the westerly maximum in the winter in the SH (Shiotani et al., 1993; Kodera and Kuroda,
35   2002), and the spring time temperature and dates of the stratospheric final warming in the SH (Newman et al., 2001; Black
and McDaniel, 2007; Hirano et al., 2016). Young et al. (2011) showed the interannual variability in the stratospheric
temperature in the tropical regions and winter extratropical regions with out-of-phase relationships and noted a close
relationship with the Rossby waves interannual variability. Kodera and Kuroda (2002) proposed a possible dynamical impact
of the 11-year solar cycle on the winter hemisphere using reanalysis data over 20 years from 1979–1998. They suggested
40   that the solar cycle controls the transition period from a radiatively controlled state of the circulation around the stratosphere
in the winter hemisphere to a dynamically controlled state and proposed a mechanism connecting the westerly jet around the
stratopause to the 11-year solar cycle through the interaction with Rossby waves.

Stationary planetary-scale Rossby waves have large amplitudes in the winter stratosphere in both hemispheres (Randel,
1988). Since stationary Rossby waves can propagate vertically in weak westerlies (Charney and Drazin, 1961), it has been
45   considered that the direct effect of stationary Rossby waves is confined to the winter hemisphere. Recent studies suggest the
presence of the interhemispheric coupling between the winter stratosphere and summer upper mesosphere through
modulation of the mesospheric circulation, which is mainly driven by gravity waves and is initiated by the stationary Rossby
wave forcing in the winter hemisphere (e.g., Becker et al., 2004; Körnich and Becker, 2010).

In the present study, the relationship of the interannual variability in the Rossby wave forcing in the SH winter to that of the
50   zonal mean fields in both hemispheres is investigated using reanalysis data over 38 years. The magnitude of the Eliassen-
Palm (EP) flux divergence is maximized around the winter extratropical stratopause, which is used here as a proxy for the
Rossby wave forcing. We perform correlation analyses between the Rossby wave forcing and zonal mean fields in both
hemispheres to clarify the dynamical coupling across the equator. The remainder of this paper is organized as follows. The
data description and method of the analysis are given in Sect. 2. The results of the analyses in terms of the Rossby wave
55   forcing characteristics in austral winter, the correlation observed in the interannual variabilities, and the relation with the
cross-equatorial flow are shown in Sect. 3. The signals in the mesosphere and the solar forcing impacts are discussed in Sect.
4. A summary and concluding remarks are given in Sect. 5.

2 Data and Methods

In this study, the Modern-Era Retrospective Analysis for Research and Applications, version 2 (MERRA-2, Geralo et al.,
60   2017) is used. The interannual variability in the zonal mean fields averaged from June to August (JJA) of 1980–2017 is the

focus period in this study. The residual mean flow $(\bar{v}^*, \bar{w}^*)$, zonal mean absolute angular momentum $\bar{M}$ and the EP flux $\boldsymbol{F} = \left(0, F^{(\phi)}, F^{(z)}\right)$ are calculated using the MERRA-2 dataset:

$$\bar{v}^* \equiv \bar{v} - \rho_0^{-1}(\rho_0 \overline{v'\theta'}/\bar{\theta}_z)_z,$$

$$\overline{w}^* \equiv \overline{w} + (a\cos\phi)^{-1}(\cos\phi\overline{v'\theta'}/\bar{\theta}_z)_\phi,$$

$$\bar{M} \equiv (z+a)(\bar{u}\cos\phi + (z+a)\Omega\cos^2\phi),$$

$$F^{(\phi)} \equiv \rho_0 a\cos\phi(u_z\overline{v'\theta'}/\theta_z - \overline{v'u'}),$$

$$F^{(z)} \equiv \rho_0 a\cos\phi\left([f - (a\cos\phi)^{-1}(\bar{u}\cos\phi)_\phi]\overline{v'\theta'}/\bar{\theta}_z - \overline{w'u'}\right),$$

where the overbar and prime denote the zonal mean and deviation from the zonal mean, respectively; u, v, and w are the zonal, meridional, and vertical wind components, respectively; f is the Coriolis parameter; θ is the potential temperature; ϕ is the latitude; a is the mean radius of the Earth; Ω is the rotation rate of the Earth; and ρ_0 is the basic density. The subscripts denote partial derivatives. The EP flux is commonly used to quantitatively diagnose Rossby wave activity. The wave forcing term in the zonal momentum equation of the transformed Eulerian-mean (TEM) system (Andrews and McIntyre, 1976) is written as the divergence of the EP flux:

$$\frac{\partial\bar{u}}{\partial t} + \bar{v}^*\left[\frac{(\bar{u}\cos\phi)_\phi}{a\cos\phi} - f\right] + \overline{w}^*\bar{u}_z = \frac{1}{\rho_0 a\cos\phi}\nabla\cdot\boldsymbol{F} + \bar{X},$$

where $\bar{X}$ is the other forcing term, such as that due to gravity waves.

3 Results

First, the interannual variability in the zonal mean fields in JJA is examined. Figures 1a and 1b show the meridional cross-section of the standard deviation of $\bar{u}$ and $\bar{T}$, respectively, over 38 years from 1980–2017. Large interannual variabilities are observed for both $\bar{u}$ and $\bar{T}$ in the SH extratropical region (90°–20°S) above a height of 30 km. There are also large interannual variabilities around the equator in the height range of 20–40 km, which is likely to be associated with the quasi-biennial oscillation.

Figure 1c shows the climatology of the root mean square of the geopotential height deviation (Z') from the zonal mean (namely, $\sqrt{\overline{Z'^2}}$), which roughly corresponds to the climatological amplitude of Rossby waves and is referred to as the wave amplitude. Large wave amplitudes are observed in the SH extratropical region, with a maximum at approximately 60°S in the height range of 45–50 km. In the NH, the wave amplitudes are small compared with those in the SH. This difference is likely because the easterly winds in the summer middle atmosphere prevent the upward propagation of stationary Rossby waves (Charney and Drazin, 1961). Figure 1d shows the climatology of EP flux divided by $\rho_0 a\cos\phi$ (arrows) and its divergence (colours). Upward propagating waves from the troposphere to the stratosphere are observed around 60°S. The waves are refracted towards the equator with height. The westward wave forcing is strong above 30 km in the SH

90   extratropical region. The wave forcing maximum is located in the latitude and height region of approximately 50–55 km (0.3–1 hPa), 50°–30°S, which is hereinafter referred to as Region A.

In the following, a correlation analysis is performed using the EP flux divergence averaged over Region A in JJA (denoted as $[\nabla \cdot \boldsymbol{F}]_A$) for each year as a proxy for the Rossby wave forcing in the SH winter. Note that $[\nabla \cdot \boldsymbol{F}]_A$ decreases as the Rossby wave forcing increases because the breaking and/or dissipation of upward propagating Rossby waves results in a

95   westward (i.e., negative) forcing. Thus, the correlation sign of the interannual variability in the zonal mean fields to $[\nabla \cdot \boldsymbol{F}]_A$ is opposite to that of the corresponding anomaly.

Figure 2a shows the correlation between the interannual variability of $[\nabla \cdot \boldsymbol{F}]_A$ and that of $\sqrt{\overline{Z'^2}}$ in the meridional cross-section. The regions with statistically significant correlations at a confidence level higher than 95% are coloured. A high correlation is observed in the SH extratropical region, where $\sqrt{\overline{Z'^2}}$ is climatologically large (Fig. 1a). In the maximum region

100   of the wave amplitude observed at approximately 60°S latitude and 45 km altitude, the absolute values of the correlation are higher than 0.8. Figure 2b shows the correlation between the interannual variabilities of $[\nabla \cdot \boldsymbol{F}]_A$ and those of $(\rho_0 a \cos\phi)^{-1} \nabla \cdot \boldsymbol{F}$. The significant correlation is not confined in Region A but is widely extended to ~10°–70°S and ~35–60 km.

Another wave forcing maximum is observed in the high latitude region of 90°–80°S above 50 km (Figure 1b). However,

105   the correlation between $\sqrt{\overline{Z'^2}}$ and the wave forcing in this region was not significant in the meridional cross-section of the winter stratosphere (not shown). It seems that this maximum is not related to the interannual variability in the Rossby waves propagating upward through the stratosphere. Thus, further analysis regarding this wave forcing in the polar region is not performed.

Figure 3a shows the correlation between the interannual variabilities in $[\nabla \cdot \boldsymbol{F}]_A$ and $\overline{T}$. Below Region A, the correlation is

110   significantly negative at 70°–30°S and positive at 30°S–30°N. Notably, the positive correlation peaks in both hemispheres of the equatorial region, in the latitude and height regions of ~10°–20° and ~30–40 km. The significant correlation exhibits a Π-shaped spatial pattern. The correlation coefficients of the positive peaks in the SH and in the NH are comparable. This indicates that the wave forcing in the SH affects the mean fields in the low latitude region of the NH. In addition, opposite-sign correlations are seen above Region A; positive correlations are observed at 70°–30°S and negative correlations are

115   observed at 30°S–30°N. The significant correlation shows a quadrupole structure that extends to the NH around Region A.

Here, the characteristics of the reanalysis dataset used in the present study should be addressed. Gelaro et al. (2017) noted that the globally averaged $\overline{T}$ in MERRA-2 changes discontinuously when new observational data are introduced into the data assimilation process. They showed that the discontinuous change is not large in the lower stratosphere but is more obvious in the upper stratosphere and mesosphere. A remarkable temperature change is observed around the stratopause before and after

120   2004, when the Earth Observation System Aura Microwave Limb Sounder (MLS) data were introduced for assimilation. To assess the effect of this reanalysis data discontinuity on the present results, the same analyses as those shown in Fig. 3a are conducted but separately for 1980–2004 and 2005–2017 (Figs. 3c and 3d, respectively). The spatial patterns of correlations,

such as the quadrupole pattern around Region A and the Π-shaped pattern in the equatorial stratosphere, are still observed for both time periods. This indicates that the change in $\bar{T}$ due to the introduction of MLS temperature has a minor impact on the
125   interannual variability related to the Rossby wave forcing in the reanalysis dataset.

Figure 3b shows the correlation between the interannual variability in $[\nabla \cdot \boldsymbol{F}]_A$ and that in $\bar{u}$. In the SH, the correlation is significantly negative at 80°–50°S and positive at 50°–20°S above 20 km. Significant correlations are also observed in the NH (0°–60°N and 35–60 km). This finding indicates that the strong wave forcing in Region A is related to a weak (strong) westerly in the SH low (high) latitude region and a strong easterly in the NH low and middle latitude regions. The
130   distribution of the correlation coefficient of $\bar{u}$ is qualitatively consistent with that of $\bar{T}$ in terms of the thermal wind balance.

The correlation of the residual mean flows $(\bar{v}^*, \bar{w}^*)$ with $[\nabla \cdot \boldsymbol{F}]_A$ is shown in Figs. 4b and 4a. Below Region A, the correlation of $\bar{w}^*$ is significantly positive at 70°–30°S, as shown in Fig. 4a. This means that $\bar{w}^*$ is downward when the wave forcing in Region A is strong. In Fig. 4b, a significantly positive correlation of $\bar{v}^*$ is observed in the latitude and height regions of 20°–60°S and 35–55 km, corresponding to the region in which the correlation of the EP flux divergence with
135   $[\nabla \cdot \boldsymbol{F}]_A$ is significant (Fig. 2b). This finding indicates that $\bar{v}^*$ is poleward where the wave forcing is strong. Interestingly, there are also significantly positive correlations of $\bar{v}^*$ at 30°S–30°N and at 35–45 km and 50–60 km. In particular, the positive correlation is high below 40 km in the NH. These spatial patterns are also consistent with the correlation of $\bar{T}$ (Fig. 3a) through the adiabatic processes associated with vertical motions. The strong wave forcing maintains a downwelling and high temperature at approximately 70°–30°S, cross-equatorial southward circulation at approximately 40 km, and upwelling
140   and low temperatures at approximately 20°S–30°N. In fact, the characteristic Π-shaped structure in the $\bar{T}$ correlation (Fig. 3a) is also seen in $\bar{w}^*$, although the spatial pattern of the correlation of $\bar{w}^*$ slopes down towards the north.

If the meridional gradient of $\bar{M}$ $(\bar{M}_y)$ is nonzero, the wave forcing is necessary to maintain the meridional circulation (Plumb and Eluszkiewicz, 1999). At low latitudes, $\bar{M}_y$ can be zero with background zonal wind shear, which permits meridional movement of air parcels even in the absence of a wave forcing (e.g., Tomikawa et al., 2008). A climatological
145   meridional cross-section of $\bar{M}$ and $\bar{M}_y$ in JJA is shown in Figure 5a. At the equator, $\bar{M}$ has a minimum at 25–30 km and a maxima at ~15 km and ~55 km. In the tropics, $\bar{M}_y$ is generally small compared with that at other latitudes.

To examine the interannual variabilities in $\bar{M}$, a composite analysis is performed with respect to the anomalies of $[\nabla \cdot \boldsymbol{F}]_A$ from the climatology. The strong (weak) wave forcing years are defined as the years with $[\nabla \cdot \boldsymbol{F}]_A$ anomalies, which are smaller (larger) than -0.5σ (0.5σ), where σ is the standard deviation of $[\nabla \cdot \boldsymbol{F}]_A$ (Fig. 5d). As a result, 13 years are chosen
150   as the strong wave forcing years (1985, 1988, 1992, 1993, 1996, 1997, 2002, 2004, 2005, 2010, 2012, 2013, and 2017) and 15 years are chosen as the weak wave forcing years (1980, 1981, 1983, 1987, 1989, 1995, 1998, 1999, 2000, 2001, 2003, 2008, 2009, 2011, and 2015). Figures 5b and 5c show the composite of $\bar{M}$ and $\bar{M}_y$ for the strong and weak wave forcing years, respectively. The absolute angular momentum around the equator at 35–40 km is small (large) when the wave forcing is strong (weak). At these altitudes, the region of small $|\bar{M}_y|$ in the strong wave forcing years extends to higher latitudes. The
155   altitudes of these variabilities are in accordance with that of the cross equatorial $\bar{v}^*$ that is correlated with $[\nabla \cdot \boldsymbol{F}]_A$ in Figure

4b. Thus, the wave forcing modifies the residual mean circulation in two ways: driving the residual mean flow in the SH and modifying the mean wind around the equator with a low $\left|\bar{M}_y\right|$.

We performed the same analysis but separately for the periods of 1980–2004 and 2005–2017 to examine the impact of the temperature discontinuity in MERRA-2 and confirmed that the results are qualitatively the same as those for 1980–2016 (not

160   shown).

4 Discussion

4.1 Relationship with previous studies

In Sect. 3, the correlation between the wave forcing in Region A ($[\nabla \cdot \boldsymbol{F}]_A$) and the zonal mean fields in the altitudes below Region A is shown. Specifically, the correlation between the interannual variabilities in $\bar{T}$ and $[\nabla \cdot \boldsymbol{F}]_A$ is

165   significantly negative at 70°–30°S and positive at 30°S–30°N below Region A. In contrast, the opposite-sign correlation is observed above Region A, namely, there is a positive (negative) correlation at 70°–30°S (30°S–30°N), which forms a quadrupolar pattern in the correlation coefficient together with the correlation below Region A. It is known that the quadrupolar pattern of the temperature anomaly appears when the stratospheric sudden warming caused by planetary wave breaking occurs in the NH (Matsuno, 1971). Since the quadrupolar structure is observed in the seasonal mean field, the

170   quadrupolar pattern of the temperature anomaly shown in the present study is not the same as the mechanism shown by Matsuno (1971). Instead, the observed quadrupolar pattern of the temperature anomalies shown by the present study can be explained as follows. When the Rossby wave forcing around Region A is strong, the anomaly of the poleward circulation with upwelling at low latitudes and downwelling at high latitudes is induced in the stratosphere below through the downward control principle (Haynes et al., 1991). These vertical flow anomalies induce adiabatic heating, which

175   corresponds to the lower part of the quadrupolar pattern. The zonal wind field is also modulated to maintain the thermal wind balance with the modulated temperature field. The westerly is weakened in the austral winter stratosphere, and the upward propagation of gravity waves with the westward phase speeds to the mesosphere is prevented. This modulation of the gravity wave propagation weakens the mesospheric meridional circulation, which induces the temperature anomalies adiabatically.

180   Körnich and Becker (2010), Karlsson and Becker (2016), and Gumbel and Karlsson (2011) showed the interhemispheric coupling in which the Rossby wave forcing in the winter hemisphere modifies the temperature around the summer polar mesopause and controls the interannual variability in the polar mesospheric clouds. This coupling is caused by the modulation of the mesospheric circulation driven by gravity waves where the propagation is affected by the mean wind change by the Rossby wave forcing in the winter hemisphere. The interhemispheric coupling shown in the present study is

185   different from that shown in previous studies but occurs in the stratosphere only by the Rossby waves, and the gravity waves are not important in the mechanism.

4.2 On the impact of the 11-year solar cycle

The relationship of the interannual variabilities in the stratosphere with the solar cycle is examined in the present study and discussed in this section. Kodera and Kuroda (2002) noted that the seasonal evolution of the winter stratopause jet is

190   considered to be the transition from a radiatively controlled state, in which the wave forcing is small and the zonal wind is roughly determined by a radiative forcing, to a dynamically controlled state, when the wave amplitude is large and radiative forcing to the zonal wind is small. They showed that the timing of this transition is largely affected by the 11-year solar cycle as well as the interannual variabilities in the wave forcing in the lower stratosphere. The proposed mechanism is as follows. During the solar maximum phase, the winter stratospheric jet remains in the radiatively controlled state for a longer period

195   due to the enhanced meridional temperature gradient between the equatorial and polar regions (Kodera and Yamazaki, 1990). Since the winter stratospheric jet remains strong during a radiatively controlled state, planetary scale Rossby waves propagating to the winter upper stratosphere are deflected from the midlatitudes. The reduced Rossby wave forcing in the midlatitude region leads to the weakening of the meridional circulation and upwelling around the equator in the stratosphere. According to this mechanism, the stratospheric interhemispheric coupling examined in the present study may be attributed to

200   the solar cycle.

The 10.7 cm solar radio flux (F10.7 index) averaged from June to August is used as the proxy for solar activity. Figure 6 shows the time series of $[\nabla \cdot \boldsymbol{F}]_A$ and the F10.7 index. The solar activity clearly exhibits an 11-year cycle oscillation. Note that the magnitude of the F10.7 index in the solar maximum phase obviously differs in each cycle, although the F10.7 index shows similar values in the solar minimum phases. The F10.7 index at the solar maximum phase at approximately 1990 is

205   large and decreases in the later maximum phases. In contrast, the wave forcing shows a clear interannual variability with similar amplitudes during the displayed time period. In the time period before 2004, which overlaps with the period analysed in Kodera and Kuroda (2002), $[\nabla \cdot \boldsymbol{F}]_A$ seems to be synchronized with the F10.7 index. The correlation is positive (0.41) but not statistically significant. In contrast, after 2004, $[\nabla \cdot \boldsymbol{F}]_A$ and the F10.7 index are roughly out of phase, although the correlation is not significant (-0.21). The correlation between $[\nabla \cdot \boldsymbol{F}]_A$ and F10.7 during the whole period is not statistically

210   significant (0.29). The change in the relation between the 11-year solar cycle and atmosphere at ~2000 was also reported in Hervig et al. (2015). They noted that the response of polar mesospheric clouds (PMCs) to the 11-year solar cycle is obvious in the 1980s and 1990s, while the PMCs response to the solar cycle is absent during 2000–2014. They discussed several possible explanations for this change observed at approximately 2000, which includes an apparent solar forcing amplification due to volcanic eruptions, namely, the eruptions of El Chichon in 1982 and Pinatubo in 1991.

215   ## 5 Summary and concluding remarks

The relationship of the interannual variabilities in the zonal mean fields and those of the Rossby wave forcing was examined using MERRA-2 reanalysis data with a focus on the interhemispheric coupling through the stratosphere. In the SH

in winter, the Rossby wave forcing is maximized in the region of 30°–50°S and 0.3–1 hPa (Region A) and shows a large interannual variability. The interannual variability in the Rossby wave forcing in this region ($[\nabla \cdot \boldsymbol{F}]_A$) is correlated with that

220   of other zonal mean fields, even in the NH stratosphere at low latitudes as well as in the SH stratosphere at nearly all latitudes. Specifically, a negative correlation of $\bar{T}$ with $[\nabla \cdot \boldsymbol{F}]_A$ at 30°S–30°N and a positive correlation of $\bar{u}$ with $[\nabla \cdot \boldsymbol{F}]_A$ at 50°S–60°N are statistically significant. Correspondingly, a significant correlation of the residual mean flow with $[\nabla \cdot \boldsymbol{F}]_A$ is observed in both the NH and the SH. The spatial pattern of the correlation suggests that the material circulation crosses the equator at an altitude of ~40 km and that the NH part of this circulation is affected by the Rossby wave forcing in the SH

225   Region A. To investigate the possible pathways of the cross-equatorial flow, we performed a composite analysis for absolute angular momentum ($\bar{M}$) by dividing it into strong and weak wave forcing years. The meridional gradient of $\bar{M}$ at ~40 km is small in the strong wave forcing years when the cross-equatorial residual mean flow is observed.

    The Rossby wave forcing in the SH stratosphere drives the residual mean circulation that connects the stratospheric zonal mean field of the SH and the NH over the equator. The cross-equatorial residual mean flow is not directly driven by the

230   Rossby wave forcing but indirectly maintained by the weak and small meridional gradient of the absolute angular momentum around the equator. Tomikawa et al. (2008) noted the interaction of the cross-equatorial flow around the stratopause and the semiannual oscillation of the zonal-mean zonal wind at the stratopause (S-SAO) on the seasonal time scale. The interannual variability in the S-SAO may play an important role in the interhemispheric coupling in the stratosphere. Details of the process of how the anomalies in the austral winter stratosphere propagate to the boreal summer

235   stratosphere should be clarified in future studies.

    The interhemispheric coupling shown in the present study occurs in the stratosphere through the modulation of the residual mean circulation and absolute angular momentum field by the Rossby wave forcing. The mechanism is different from the interhemispheric coupling through the mesosphere caused by the modulation of gravity waves.

Data availability.

240   The MERRA-2 dataset is provided by NASA's Global Modelling and Assimilation Office (https://gmao.gsfc.nasa.gov/). The F10.7 index in the OMNI 2 dataset is used in the present study. The OMNI data were obtained from the GSFC/SPDF OMNIWeb interface at https://omniweb.gsfc.nasa.gov.

Acknowledgements.

    We greatly appreciate Kunihiko Kodera for his helpful comments and discussions. This work was supported by JST

245   CREST JPMJCR1663. All figures in the present study are drawn using Dennou Club Library (DCL).

References

Andrews, D. G. and McIntyre, M. E.: Planetary Waves in Horizontal and Vertical Shear: The Generalized Eliassen-Palm Relation and the Mean Zonal Acceleration, J. Atmos. Sci., 33(11), 2031–2048, doi:10.1175/1520-0469(1976)033<2031:PWIHAV>2.0.CO;2, 1976.

250   Baldwin, M. P. and Dunkerton, T. J.: Quasi-biennial modulation of the southern hemisphere stratospheric polar vortex, Geophys. Res. Lett., 25(17), 3343–3346, doi:10.1029/98GL02445, 1998.

Becker, E., Müllemann, A., Lübken, F.-J., Körnich, H., Hoffmann, P. and Rapp, M.: High Rossby-wave activity in austral winter 2002: Modulation of the general circulation of the MLT during the MaCWAVE/MIDAS northern summer program, Geophys. Res. Lett., 31(24), doi:10.1029/2004GL019615, 2004.

255   Black, R. X. and McDaniel, B. A.: Interannual Variability in the Southern Hemisphere Circulation Organized by Stratospheric Final Warming Events, J. Atmos. Sci., 64(8), 2968–2974, doi:10.1175/JAS3979.1, 2007.

Butchart, N.: The Brewer-Dobson circulation, Rev. Geophys., 52(2), 157–184, doi:10.1002/2013RG000448, 2014.

Charney, J. G. and Drazin, P. G.: Propagation of planetary-scale disturbances from the lower into the upper atmosphere, J. Geophys. Res., 66(1), 83–109, doi:10.1029/JZ066i001p00083, 1961.

260   Gelaro, R., McCarty, W., Suárez, M. J., Todling, R., Molod, A., Takacs, L., Randles, C. A., Darmenov, A., Bosilovich, M. G., Reichle, R., Wargan, K., Coy, L., Cullather, R., Draper, C., Akella, S., Buchard, V., Conaty, A., da Silva, A. M., Gu, W., Kim, G.-K., Koster, R., Lucchesi, R., Merkova, D., Nielsen, J. E., Partyka, G., Pawson, S., Putman, W., Rienecker, M., Schubert, S. D., Sienkiewicz, M. and Zhao, B.: The Modern-Era Retrospective Analysis for Research and Applications, Version 2 (MERRA-2), J. Climate, 30(14), 5419–5454, doi:10.1175/JCLI-D-16-0758.1, 2017.

265   Gumbel, J. and Karlsson, B.: Intra- and inter-hemispheric coupling effects on the polar summer mesosphere, Geophys. Res. Lett., 38(14), doi:10.1029/2011GL047968, 2011.

Hervig, M. E., Berger, U. and Siskind, D. E.: Decadal variability in PMCs and implications for changing temperature and water vapor in the upper mesosphere, J. Geophys. Res. Atmos., 121(5), 2383–2392, doi:10.1002/2015JD024439, 2016.

Hirano, S., Kohma, M. and Sato, K.: A three-dimensional analysis on the role of atmospheric waves in the climatology and

270   interannual variability of stratospheric final warming in the Southern Hemisphere, J. Geophys. Res. Atmos., 121(14), 8429–8443, doi:10.1002/2015JD024481, 2016.

Holton, J. R. and Tan, H.-C.: The Influence of the Equatorial Quasi-Biennial Oscillation on the Global Circulation at 50 mb, J. Atmos. Sci., 37(10), 2200–2208, doi:10.1175/1520-0469(1980)037<2200:TIOTEQ>2.0.CO;2, 1980.

Karlsson, B. and Becker, E.: How Does Interhemispheric Coupling Contribute to Cool Down the Summer Polar

275   Mesosphere?, J. Climate, 29(24), 8807–8821, doi:10.1175/JCLI-D-16-0231.1, 2016.

Kodera, K. and Kuroda, Y.: Dynamical response to the solar cycle, J. Geophys. Res., 107(D24), ACL 5-1, doi:10.1029/2002JD002224, 2002.

Kodera, K. and Yamazaki, K.: Long-term Variation of Upper Stratospheric Circulation in the Northern Hemisphere in December, J. Meteorol. Soc. Jpn., 68(1), 101–105, doi:10.2151/jmsj1965.68.1_101, 1990.

280   Körnich, H. and Becker, E.: A simple model for the interhemispheric coupling of the middle atmosphere circulation, Adv. Space Res., 45(5), 661–668, doi:10.1016/j.asr.2009.11.001, 2010.

Matsuno, T.: A Dynamical Model of the Stratospheric Sudden Warming, J. Atmos. Sci., 28(8), 1479–1494, doi:10.1175/1520-0469(1971)028<1479:ADMOTS>2.0.CO;2, 1971.

Newman, P. A., Nash, E. R. and Rosenfield, J. E.: What controls the temperature of the Arctic stratosphere during the

285   spring?, J. Geophys. Res., 106(D17), 19999–20010, doi:10.1029/2000JD000061, 2001b.

Okamoto, K., Sato, K. and Akiyoshi, H.: A study on the formation and trend of the Brewer-Dobson circulation, J. Geophys. Res., 116(D10), doi:10.1029/2010JD014953, 2011.

Plumb, R. A. and Eluszkiewicz, J.: The Brewer–Dobson Circulation: Dynamics of the Tropical Upwelling, J. Atmos. Sci., 56(6), 868–890, doi:10.1175/1520-0469(1999)056<0868:TBDCDO>2.0.CO;2, 1999.

290   Randel, W. J.: The seasonal evolution of planetary waves in the southern hemisphere stratosphere and troposphere, Q. J. R. Meteorol. Soc., 114(484), 1385–1409, doi:10.1002/qj.49711448403, 1988.

Randel, W. J., Wu, F. and Stolarski, R.: Changes in Column Ozone Correlated with the Stratospheric EP Flux, J. Meteorol. Soc. Jpn., 80(4B), 849–862, doi:10.2151/jmsj.80.849, 2002.

Sato, K. and Nomoto, M.: Gravity Wave–Induced Anomalous Potential Vorticity Gradient Generating Planetary Waves in

295   the Winter Mesosphere, J. Atmos. Sci., 72(9), 3609–3624, doi:10.1175/JAS-D-15-0046.1, 2015.

Shiotani, M., Shimoda, N. and Hirota, I.: Interannual variability of the stratospheric circulation in the southern hemisphere, Q.J.R. Meteorol. Soc., 119(511), 531–546, doi:10.1002/qj.49711951110, 1993.

Tomikawa, Y., Sato, K., Watanabe, S., Kawatani, Y., Miyazaki, K. and Takahashi, M.: Wintertime temperature maximum at the subtropical stratopause in a T213L256 GCM, J. Geophys. Res., 113(D17), doi:10.1029/2008JD009786, 2008.

300   Tung, K. K. and Kinnersley, J. S.: Mechanisms by which extratropical wave forcing in the winter stratosphere induces upwelling in the summer hemisphere, J. Geophys. Res., 106(D19), 22781–22791, doi:10.1029/2001JD900228, 2001.

Yamashita, Y., Akiyoshi, H. and Takahashi, M.: Dynamical response in the Northern Hemisphere midlatitude and high-latitude winter to the QBO simulated by CCSR/NIES CCM, J. Geophys. Res., 116(D6), doi:10.1029/2010JD015016, 2011.

Young, P. J., Thompson, D. W. J., Rosenlof, K. H., Solomon, S. and Lamarque, J.-F.: The Seasonal Cycle and Interannual

305   Variability in Stratospheric Temperatures and Links to the Brewer–Dobson Circulation: An Analysis of MSU and SSU Data, J. Climate, 24(23), 6243–6258, doi:10.1175/JCLI-D-10-05028.1, 2011.
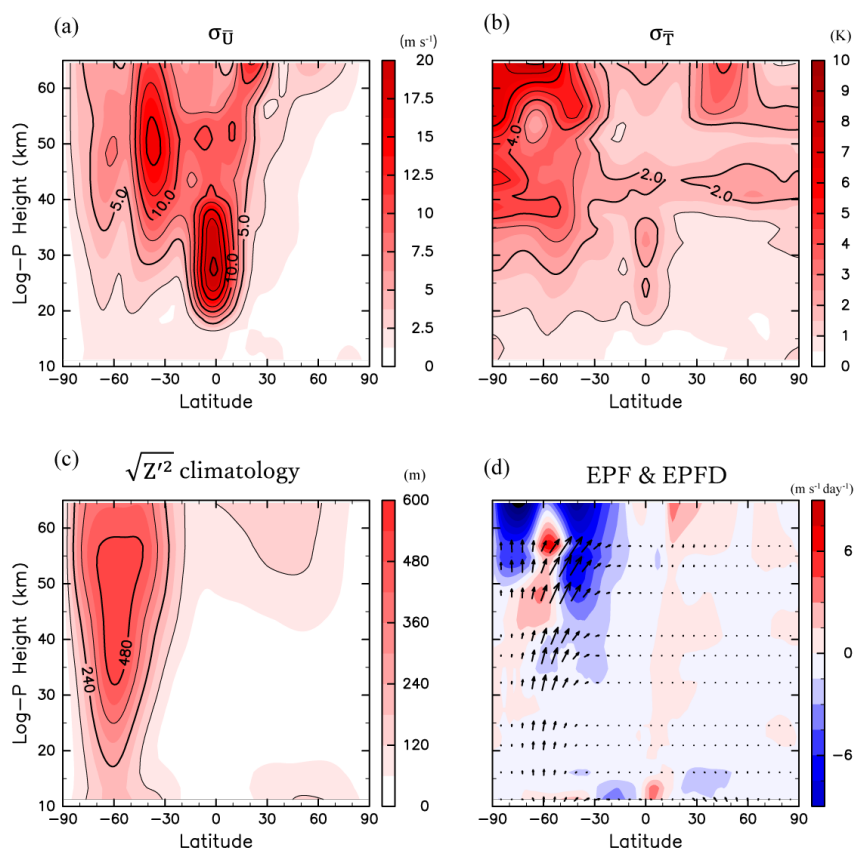
Figure 1: Meridional cross-sections of the standard deviation of (a) $\bar{u}$ (m s⁻¹) and (b) $\bar{T}$ (K) from the climatology, climatology of (c) $\sqrt{\overline{Z'^2}}$ (m), and (d) EPF (vector) and EPFD (colour, m s⁻¹ day⁻¹); the contour intervals are (a) 1 m s⁻¹, (b) 2.5 K, and (c) 120 m, respectively.
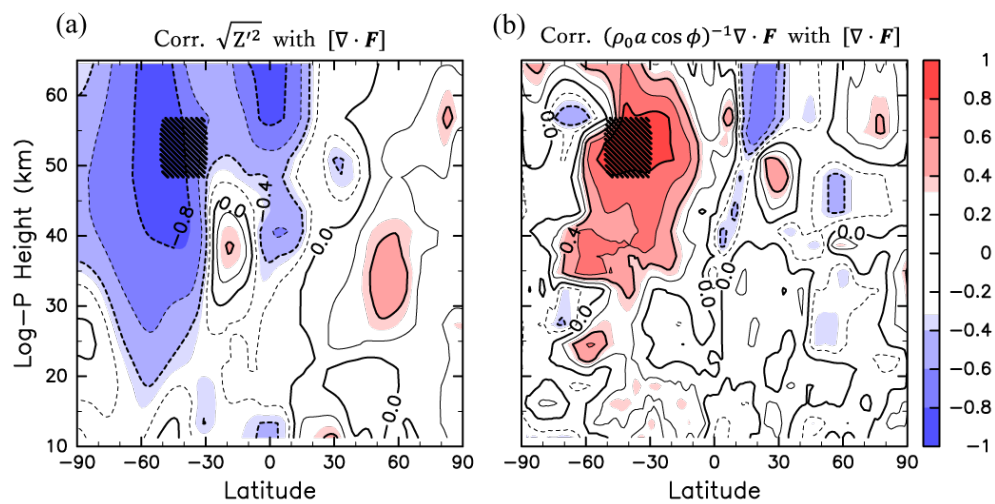
Figure 2: Meridional cross-sections of the correlation coefficient of $[\nabla \cdot \boldsymbol{F}]_A$ with (a) $\sqrt{\overline{Z'^2}}$ and (b) $(\rho_0 a \cos\phi)^{-1} \nabla \cdot \boldsymbol{F}$ for JJA of 1980–2017. Contour intervals are 0.2. Region A is indicated by hatching.
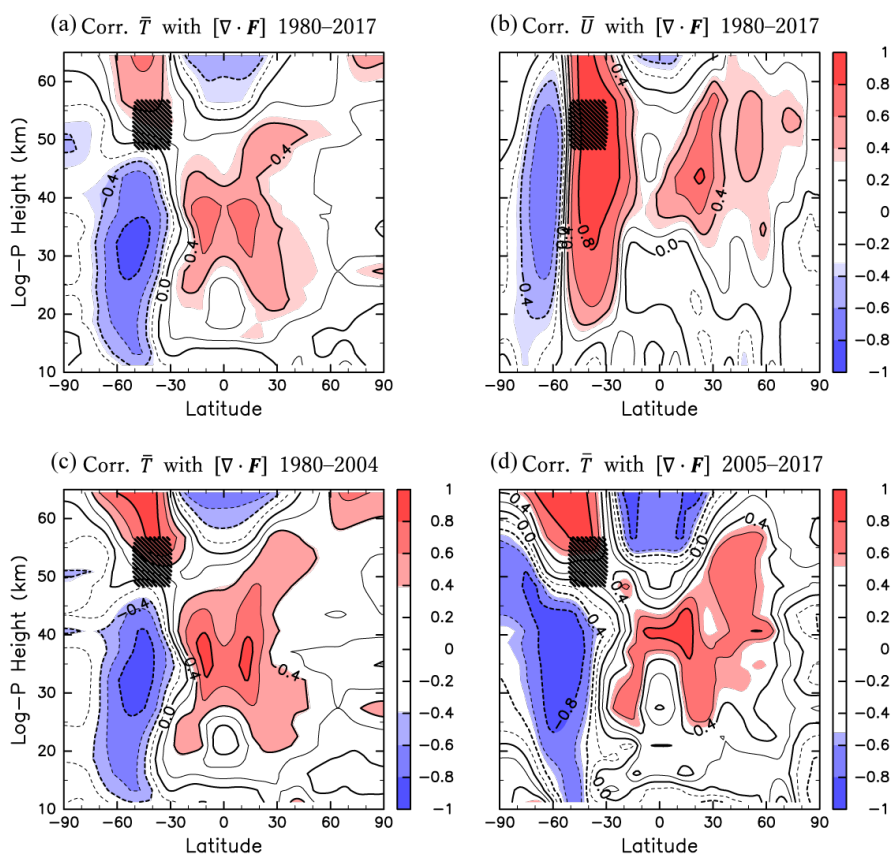
Figure 3: Same as in Fig. 2 but for the correlations of $[\nabla \cdot F]_A$ with (a) $\overline{T}$ (1980–2017), (b) $\overline{u}$ (1980–2017), (c) $\overline{T}$ (1980–2004), and (d) $\overline{T}$ (2005–2017).

320
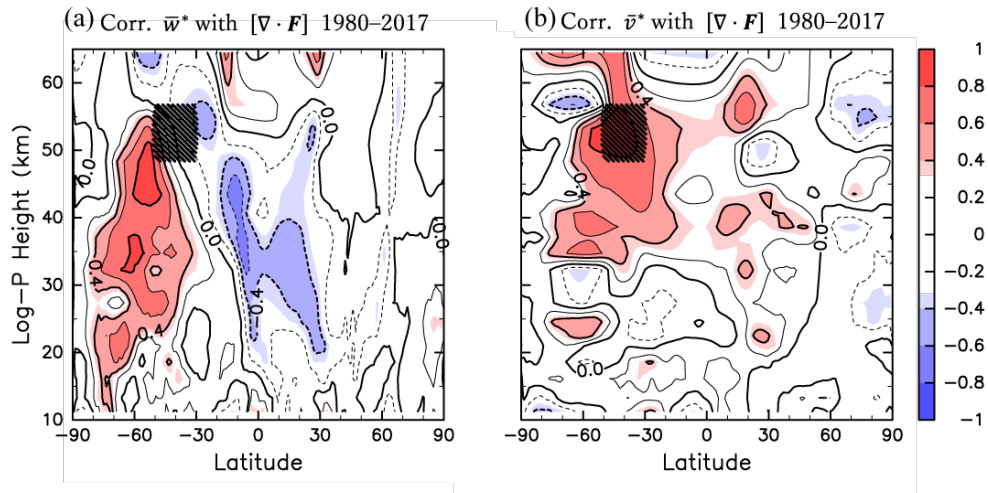
Figure 4: Same as in Fig. 2 but for the correlations of $[\nabla \cdot F]_A$ with (a) $\overline{w}^*$ (1980–2017) and $\overline{v}^*$ (1980–2017).
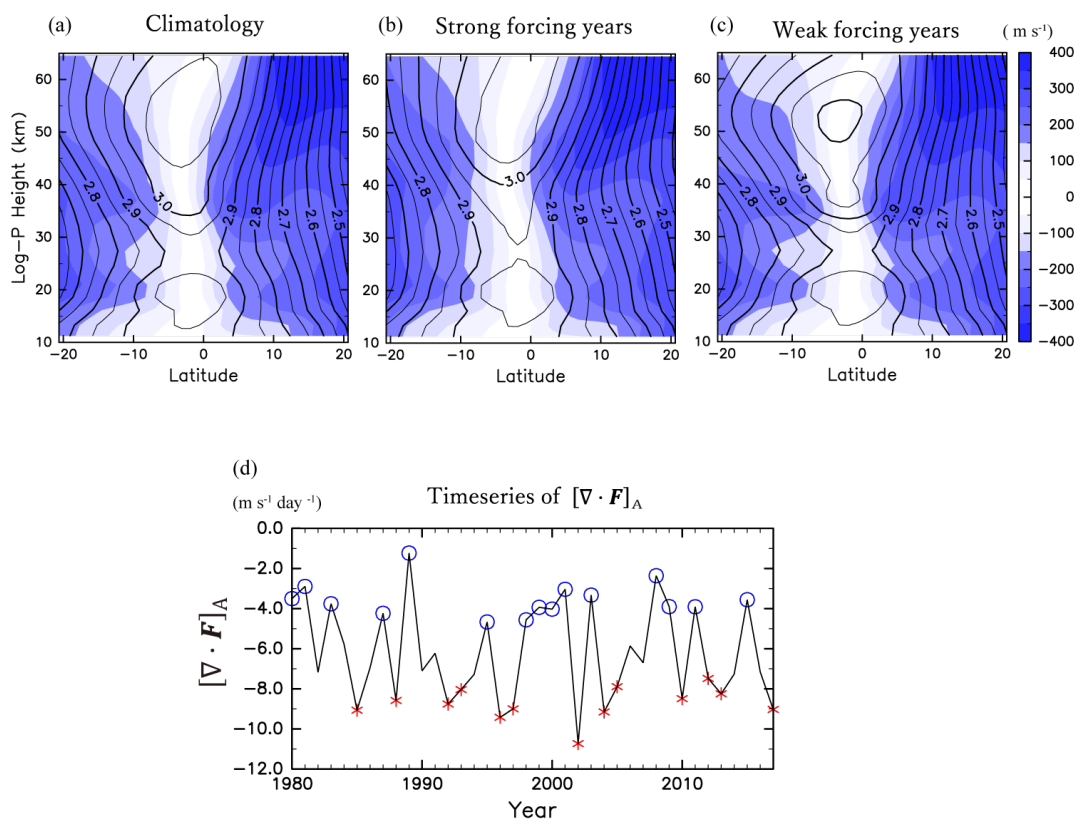
325   Figure 5: Meridional cross-sections of the (a) climatology of absolute angular momentum $\bar{M}$ (contours, 10^9 m^{2}s^{-1}) and its meridional gradient $\bar{M}_y$ (colours, m s^{-1}) for 1980–2017, (b) composite for the strong wave forcing, and (c) composite for the weak wave forcing. Contour intervals are 5×10^7 m^2 s^{-1}. (d) Time series of $[\nabla \cdot F]_A$. The red and blue marks indicate the years used for (b) and (c), respectively.
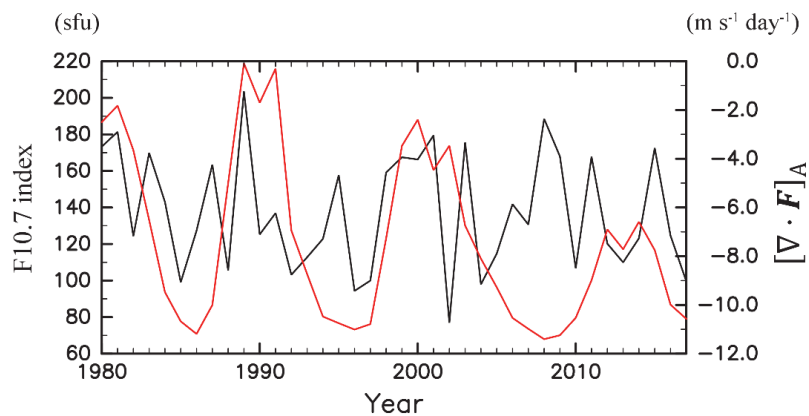
330

Figure 6: Time series of the JJA mean F10.7 index (red, sfu = 10^{-22} W m^{-2} Hz^{-1}) and $[\nabla \cdot \boldsymbol{F}]_A$ (black, m s^{-1} day^{-1}) for 1980–2017.